Focal-Plane Arrays with Improved Scan Capabilities

Focal-Plane Arrays With Improved Scan Capabilities

Aleksei Dubok and A. Bart Smolders, *Senior Member, IEEE*,

***Abstract*— This article investigates the limits of focal-plane array (FPA) technology by studying a double-reflector antenna system with wide-angle scan capabilities. The proposed reflector configurations are analyzed in terms of effective isotropic radiated power (EIRP) maximization, minimization of the required total number of array elements for a wide-scan range, and the highest number of simultaneously active array elements of the phased-array feed. Presented configurations have capabilities to operate in the scan range up to ±30° in azimuth (±35 beamwidths scan) and ±3° in elevation. It has been demonstrated how different optimizations could allow to build systems with varying performance in terms of the key operation parameters, such as array size, EIRP, and the number of active array elements. A detailed analysis is provided that demonstrates the potential applicability of this concept in future millimeter-wave (mm-wave) applications.**

***Index Terms*— 5G, 6G, antenna array, focal-plane arrays (FPAs), millimeter-wave (mm-wave), reflector antennas, reflector modeling, wide-scan range, wireless communications.**

I. Introduction

FOCAL-PLANE arrays (FPAs) form a promising antenna technology allowing to combine the benefits of reflector-based systems that provide high antenna directivities and phased arrays, which are traditionally used for multibeam and electronic beam-scanning applications. As a result, FPAs are widely used in radio astronomy [1], satellite and point-to-point communications [2], and low-cost Ka-band (30–40 GHz) multifunction radars [3]. An interesting area of research is to investigate if FPAs can be used to realize base stations (also referred to as remote radio units) for future millimeter-wave (mm-wave) wireless communications infrastructure to meet the demands of 5G and beyond.

One of the main limiting factors of the existing solutions for mm-wave 5G base stations is the limited range and insufficient power budget due to the lack of system directivity [4], [5]. This leads to the necessity to use a huge number of array elements when using traditional phased array-based systems. The FPA concept could solve those issues if it would be possible to design the FPA systems with wide-scan capabilities. The proposed concept should demonstrate an improved performance compared with the traditionally used phased arrays in terms of required array elements.

Traditionally, reflector systems have limited scanning potential and are dedicated to applications that required high directivity within an extremely narrow angular section. Classical reflectors focus the received wave front on a relatively small spot in the focal plane. Multibeam operation with such reflectors is normally done by placing a few separate feeds in the focal plane. This approach only works well over a relative small angular range, since the point in the focal plane on which the energy is focused deviates strongly with increasing offset angle [6], [7], even for small offset angles with respect to broadside.

The use of arrays as feeds for reflector systems allows scanning the main beam over a wider angular range. At the same time, the focusing properties of traditional reflectors significantly deteriorate during scanning. As a result, only a small number of active array elements are typically used in the focal plane [6], [8], [9], [10]. This limits the number of simultaneously available beams or scan range [11], [12] and limits the achievable effective isotropic radiated power (EIRP) [13], [14], [15]. At the same time, the required array size grows dramatically with increased scan range requirements. Nevertheless, the array feed could compensate the reflector defocusing to achieve a high level of EIRP over the entire scan range. At the same time, mutual reposition of the reflector and array feed, so-called axial displacement of the array, allows to increase the number of involved array elements within the required scan range [16]. Moreover, the previously presented paper [10] demonstrates that it is possible to optimize the scan performance of FPAs and to improve its scan capabilities. In [10], we have investigated a complex offset double-reflector system, as illustrated in Figs. 1 and 2, which provides a scan range of ±20° in the azimuth plane.

In this article, we will bring the concept of [10] to a next level by addressing the following research challenges:

1) investigation of the maximum achievable scan range that FPA systems can provide, in particular for the double-reflector model with wide-scan capabilities;
2) decrease the beam deviation in the focal plane region during scanning;
3) investigation of the most crucial factors of wide scanning FPAs, such as the array size required to provide

Manuscript received 5 October 2021; revised 20 September 2022; accepted 25 October 2022. Date of publication 8 November 2022; date of current version 19 January 2023. This work was supported by The Netherlands Organization for Scientific Research (NWO) Technology Foundation through the Framework of the Project FREEBEAM. *(Corresponding author: Aleksei Dubok.)*

The authors are with the Electrical Engineering Department, Eindhoven University of Technology, 5600 MB Eindhoven, The Netherlands (e-mail: A.Dubok@tue.nl; A.B.Smolders@tue.nl).

Color versions of one or more figures in this article are available at https://doi.org/10.1109/TAP.2022.3218931.

Digital Object Identifier 10.1109/TAP.2022.3218931

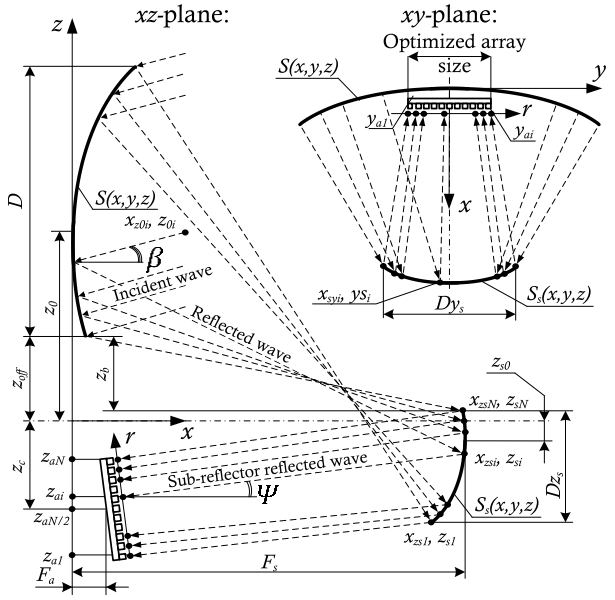

Fig. 1. Complex offset double-reflector model [10].

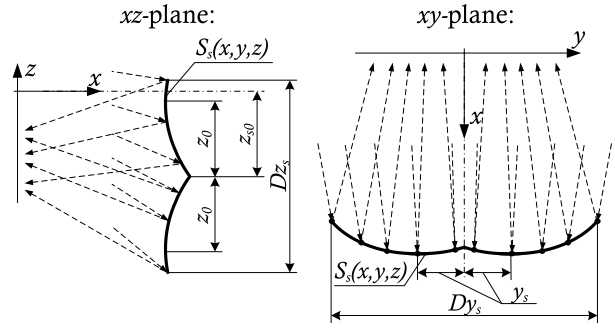

Fig. 2. Complex offset double-reflector model with discontinuities of the 3-D offset reflector [10].

increased scanning capabilities, effects of different sub-reflector sizes and limits in case of 2-D scanning, and the ratio between the number of active array elements versus the total number of array elements;

4) explore configurations with a wide illumination area of the array to maximize the EIRP;
5) develop a wideband FPA system, operating over a wide operational bandwidth in K- and Ka-band between 20 and 40 GHz.

Similar to [10], we will work at a frequency of 30 GHz. It is important to note that the results of array size minimization are not only related to a certain scan range, but also to the reflector sizes. It is obviousthat for identical operational conditions, such as the scan range or reflector type, a larger main reflector could provide a higher directivity.

The structure of this article is as follows. Section II describes the concept of a complex offset double-reflector model optimized for different optimization goals. The situation with sub-reflectors is more complicated and is discussed in Section III where we will show reflector optimization results for a minimum array size for different sizes of the sub-reflectors. Both length and height of the sub-reflectors have been varied for those optimizations. Section IV discusses the most challenging optimization of the required array size for 2-D scanning with fixed sizes of the reflectors. In addition to the previously used azimuth scan range up to ±30° corresponding to ±35 beamwidths scan for a 0.8 m reflector at 30 GHz [10], an additional elevation scan range up to ±3° is demonstrated.

II. Double-Reflector Antenna With Improved Scan Capabilities

The traditional problems for FPAs with a wide-scan range are twofold: 1) we need to use a relatively large array to compensate for the beam deviation while scanning and 2) we need to use a sufficient number of active array elements to meet the required EIRP level. At the same time, the array elements are costly in such systems, and the idea is to use them as much as possible. It is required to have a mechanism to connect the defined properties of the system, required directivity, scan range, and overall dimensions, with the properties of the array, such as array size and the number of involved elements. Knowing such relations, it is possible to find a way to control, optimize, and improve the FPA properties over the entire scan range. Such a method as a strictly deterministic mathematical algorithm has been proposed by Dubok et al. [10]. Our model uses a geometrical optics (GO) approach, which applies Snell's law according to [17], [18], and [19]. When we describe the reflector surface as a mathematical function and divide the surface into a finite number of points, it is possible to find the normal at each point of the reflector. Based on Snell's law, the reflected wave in each reflector point can be calculated. In this way, the field distribution in the array plane can be determined, resulting in a cost function used in our optimization process.

The concept presented in [10] investigates a complex offset double-reflector model (Figs. 1 and 2) for a scan range of ±20° in the azimuth plane without scanning in the elevation plane. The size of the array in the elevation plane has been fixed to 4 cm, and in the azimuth plane, the size is subject of optimization; see Fig. 1. The main reflector size is 0.8 m diameter, which provides a maximum directivity of 48 dBi at 30 GHz. The maximum sub-reflector size is limited to 83 × 30 cm. The obtained configuration has been used to construct a prototype for experimental validation (see Fig. 3). The simulation and measurement results confirm the proposed method and prove that the optimization algorithm works well and allows to significantly improve the performance within a predefined scan range, such as array size minimization and the maximization of the ratio of active array elements in FPAs. Nevertheless, the question about the applicability of the proposed method for other optimization goals (beyond ±20° in azimuth and with additional limited scan in the elevation plane) has not been disclosed. In addition, other scan range requirements could also lead to other optimal configurations. Thus, in the frame of this article, additional investigations are done.

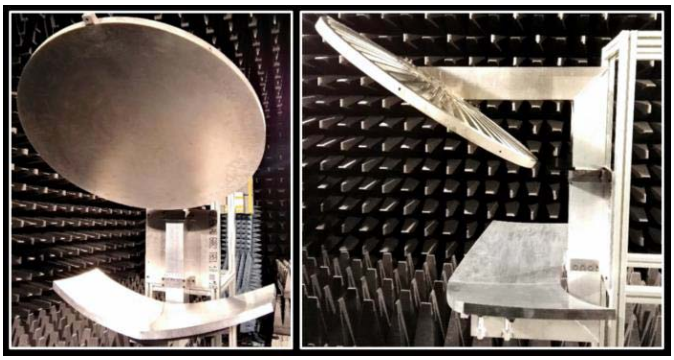

Fig. 3. Photograph of the prototype using a complex offset double-reflector setup [10].

In the proposed configuration of paper [10], the reflector elevation incline angle β acts as one of the geometrical parameters optimized by GO [20], [21]; see Fig. 1. This incline is also visible in the photograph of the prototype in Fig. 3. It is important to note that this parameter has been limited during optimization with a maximum value for up to 40°. It is obvious that with a higher elevation incline, the effective area of the main reflector will be lower, reduced according to $\cos\beta$. As a result, the directivity of the reflector system will degrade with increasing β. At the same time, as will be demonstrated in this article, the introduction of this elevation aspect could improve the optimization results for reflector minimization during scanning. To find a balanced solution within this article, the reflector optimizations have been done for three different maximum values of β defined in the optimization code. Similar to [10], one compilation of optimization limits the maximum value for β to 40°, which is related to a 23.4% potential loss of directivity. Two other cases limit the maximum β to 20° and 0°, which is equivalent to a potential loss of directivity of 6% and 0%, respectively.

In [10], the optimization has been done for a "complex" or multivariable set of optimization goals. This set is a combination of the minimum required array size to realize a certain scan range and the maximization of the ratio of active versus non-active array elements. Depending on the FPA application, different optimization goals could be more relevant than others. Thus, to cover the technology applicability, it is necessary to investigate optimization goals that improve a certain aspect of the FPA. For example, the overall number of array elements could be minimized by minimizing the array dimension during operation within the required scan range. Nevertheless, the foundation stone is the optimization of the ratio of active versus total number of array elements of the FPA within the scan range.

We will introduce a new parameter RATA, which represents the Ratio between the number of Active array elements contributing to the reflector illumination for a certain scan angle to the Total number of Array elements [10]. The RATA will vary over the scan range, between the minimum and maximum values, as illustrated in Fig. 4. A high RATA results in a high EIRP level.

Fig. 4 presents the typical situation for classical prime-focused reflectors. For larger scan angles, the focusing

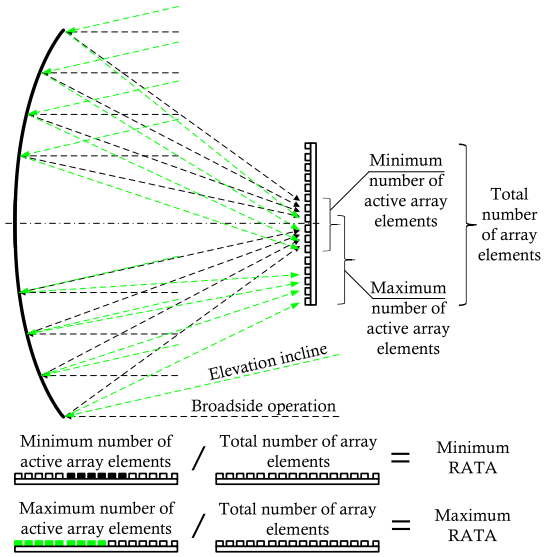

Fig. 4. Maximum and minimum RATA of FPA within the scan range.

properties of the reflector deteriorate, and the beam is broadened in the array plane. As a result, the number of active array elements is at its minimum for broadside operation and increases with scanning, reaching a maximum at the maximum scan incline.

For classical prime-focused reflectors, the field distribution in the focal plane is presented as an Airy pattern with ring-like distribution. The aperture efficiency if found by integrating the electric field on the focal plane along the aperture and normalizing it to the total power received by the reflector [22]. For standard reflector configurations, an aperture efficiency of 100% for a given field distribution in the array plane can only be achieved by using an infinitely large aperture radius. The array element is considered active if it is included in the aperture radius related to an aperture efficiency of 80% [8]. It is obvious that for different reflector configurations that operate within a defined scan range, the field distribution in the focal plane could take various forms. Nevertheless, the definition of "active array element" remains relevant [10].

Within this article, we will extend the optimization method of the paper [10] by investigating in Section II-A how the multivariable optimization can be extended to more extreme scan ranges up to ±30°. Next to this, alternative optimization goals will be investigated in Sections II-B–II-E. Table I summarizes all optimizations described in Section II. Section II-F summarizes the results achieved by different optimization methods.

For all optimizations, we have used a fixed array size of 4 cm in the elevation plane. The main reflector size is 0.8 m in diameter, and the maximum allowed sub-reflector size is 100 × 45 cm.

A. Multivariable Optimization Goal

Within this subparagraph, the optimization results for 21 different reflectors configurations for a multivariable optimization goal are presented. The configurations vary based on the

TABLE I

SUMMARY OF OPTIMIZATION DESCRIBED IN SECTION II

Section	Optimization name	Optimization description
II-A	Multi-variable optimization goal	Combination of the minimum required array size and the maximization of the RATA, like in [10]
II-B	Maximization of EIRP within defined scan range	Maximum RATA. Second optimization factor is the array size minimization
II-C	Minimum RATA	Maximizing the minimum RATA that can occur in a certain scan range (Fig. 4)
II-D	Maximization of EIRP and the minimum RATA	The combination of goals of Sec.II-B and C, by maximizing the peak EIRP for broadside operation and improve the minimum RATA over the entire scan range
II-E	Array size minimization	The minimum array size which could serve the required scan range

TABLE II

OPTIMIZATION RESULTS WITH MULTIVARIABLE GOAL FOR THE COMPLEX OFFSET DOUBLE-REFLECTOR MODEL FOR $\beta = 40°$

	Azimuth scan range, deg						
	0	±5	±10	±15	±20	±25	±30
Array size, cm	0.2	6.2	11.6	20.5	21.7	27.7	40.63
Maximum RATA, %	100	99.53	95.73	44.07	61.25	50.66	20.75
Minimum RATA, %	100	35.75	24.91	6.45	5.27	5.05	6.48

TABLE III

OPTIMIZATION RESULTS WITH MULTIVARIABLE GOAL FOR THE COMPLEX OFFSET DOUBLE-REFLECTOR MODEL FOR $\beta = 20°$

	Azimuth scan range, deg						
	0	±5	±10	±15	±20	±25	±30
Array size, cm	0.3	9.9	20.5	34.4	43.2	79.7	121.3
Maximum RATA, %	100	61.48	62.46	39.65	61.53	41.71	42.14
Minimum RATA, %	100	3.15	0.99	2.18	6.73	26.60	34.36

maximum required scan range and are based on the maximum allowed angle β of the reflector configuration; see Fig. 1. The scan range starts from 0° (broadside operation) and increases up to ±30° maximum. Each scan range corresponds to different optimized reflector configurations. The multivariable set of optimization goals combines minimum array size and maximization of the RATA. The optimization set combines those goals with the same weighting coefficients as in paper [10].

Table II contains the optimization results of the complex offset double-reflector models for β limited to 40°, and Tables III and IV for 20° and 0°, respectively.

A comparison between reflector configurations with different limits on β is presented in Fig. 5 for varying array sizes and in Fig. 6 for the RATA.

An azimuth scan range of 0° corresponds to broadside operation only. If we do not scan, the minimum and maximum RATA values are always equal to 100%, since there is no beam deviation related to scanning. As a result, for broadside, we only minimize the required array size.

TABLE IV

OPTIMIZATION RESULTS WITH MULTIVARIABLE GOAL FOR THE COMPLEX OFFSET DOUBLE-REFLECTOR MODEL FOR $\beta = 0°$

	Azimuth scan range, deg						
	0	±5	±10	±15	±20	±25	±30
Array size, cm	0,04	24,9	52,3	80,1	110	154,2	210,9
Maximum RATA, %	100	3.63	7.75	10.76	13.74	13.33	24.59
Minimum RATA, %	100	2.67	4.04	4.66	5.75	1.93	8.56

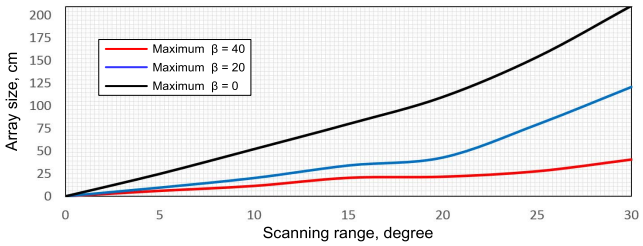

Fig. 5. Array size for the complex offset double-reflector model optimized for a multivariable goal.

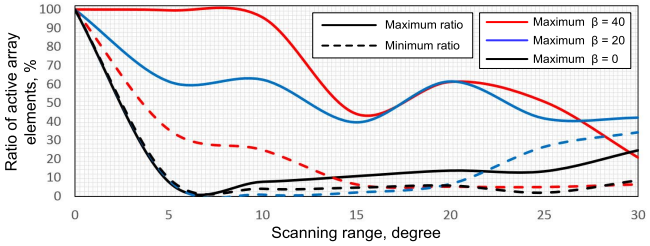

Fig. 6. RATA for the complex offset double-reflector model optimized for a multivariable goal.

In case of scanning, it is possible to optimize the RATA of the reflector configuration within a defined scan range. Each scan range corresponds to different optimized reflector configurations and to different minimum and maximum RATA values. For example, the configuration optimized to operate within a scan range of ±20° will have a certain minimum and maximum RATA within this ±20° range. The configuration optimized to work within ±30° is going to be different and will have other minimum and maximum RATA values; see Tables II–IV.

When only optimizing the maximum RATA, we improve the best-case operation, the best-case peak EIRP. At other scan angles, the RATA might be much lower. On the other hand, when we only optimize the minimum RATA, we improve the RATA over the whole scan range. Both optimization goals could be combined with a certain proportion. Those could be interesting for radar application, since system sensitivity could be optimized in a certain direction and balanced with a minimum required sensitivity in other directions.

Table II contains the results of the reflector optimization for ±20° scanning with a limit of 40° of the maximum β; see

TABLE V

OPTIMIZATION RESULTS FOR EIRP MAXIMIZATION USING A MULTIVARIABLE GOAL FOR THE COMPLEX OFFSET DOUBLE-REFLECTOR MODEL FOR $\beta = 40°$

	Azimuth scan range, deg					
	±5	±10	±15	±20	±25	±30
Array size, cm	**6.82**	**8.97**	**13.66**	**18.062**	**26.69**	**40.6**
Maximum RATA, %	**100**	**100**	**100**	**100**	**100**	**100**
Minimum RATA, %	2.14	11.06	6.63	9.84	29.41	56.84

Fig. 5. This is the same optimization requirement as for the proposed configuration in paper [10]. The required minimum array size, which was 28 cm in paper [10] based on physical optics (PO) simulations in GRASP [23], is now reduced to 21.7 cm in this article based on GO optimization code. The slight improvement can be explained by the fact that in [10], the sub-reflector length has been limited to 83 cm due to the prototype production restrictions, while in this article, the maximum dimension of sub-reflector size has been limited to 1 m.

From Fig. 5, it is clear that the required array size is increasing with increased scan range quite linearly. In addition, there is a clear difference versus incline angle. A limit of β to 20° results in an increase of the required array size of almost a factor of 3 for a scan range of ±30° as compared with the situation of a 40° limit of β. In case $\beta = 0°$, the required array size is more than five times larger as compared with the maximum value for $\beta = 40°$. From Fig. 6, we can observe a similar trend for the RATA. Both the maximum and the minimum RATA values show a degradation with strict limits on β and degradation for wider scan ranges. Thus, it is obvious that some degradation in directivity could be acceptable to significantly reduce the array size and, as a result, the number of array elements for a wide-scan range.

B. Maximization of EIRP Within Defined Scan Range

Within this section, the optimization results for another 21 different reflectors configurations when maximizing the EIRP are presented. As in the previous case, the configurations vary based on the maximum required scan range and are based on the maximum allowed β angle.

For this optimization, it is possible to create a situation where the entire array is active for a certain scan angle, so we could achieve a maximum RATA of 100%. In this situation, a second optimization factor will be used that will minimize the overall array dimension if the maximum RATA achieves 100%.

Within this article, we investigate the use case when the maximum RATA is optimized for broadside operation. If the maximum RATA for this optimization achieves 100%, this means that this configuration has all elements active for broadside operation and at the same time capable to provide scanning within the defined scan range (of course with less RATA than 100% for non-broadside operation) and achieves all of that with a minimum required array size. An example of such a system is presented in Fig. 7.

Table V contains the optimization results of complex offset double-reflector models for β limited to 40°, and Tables VI and VII for 20° and 0°, respectively.

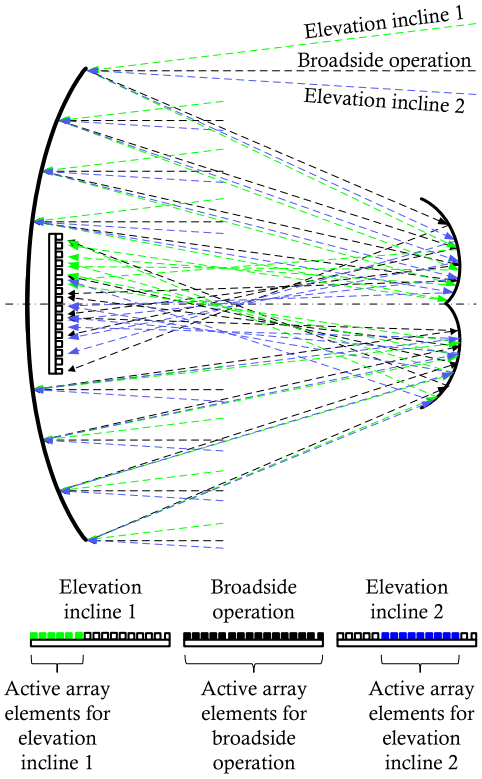

Fig. 7. Illustration of an FPA with scanning capabilities and with the maximum RATA equal to 100% for broadside operation.

TABLE VI

OPTIMIZATION RESULTS FOR THE EIRP MAXIMIZATION USING A MULTIVARIABLE GOAL FOR THE COMPLEX OFFSET DOUBLE-REFLECTOR MODEL FOR $\beta = 20°$

	Azimuth scan range, deg					
	±5	±10	±15	±20	±25	±30
Array size, cm	**9.3**	**17**	**35.8**	**42.6**	**89.8**	**118.2**
Maximum RATA, %	**100**	**100**	**100**	**100**	**100**	**100**
Minimum RATA, %	3.12	4.03	34.47	24.66	52.09	49.94

TABLE VII

OPTIMIZATION RESULTS FOR THE EIRP MAXIMIZATION USING A MULTIVARIABLE GOAL FOR THE COMPLEX OFFSET DOUBLE-REFLECTOR MODEL FOR $\beta = 0°$

	Azimuth scan range, deg					
	±5	±10	±15	±20	±25	±30
Array size, cm	**9.67**	**46.7**	90.6	102.5	162.2	210.8
Maximum RATA, %	**100**	**100**	**89.61**	**74.88**	**45.10**	**24.62**
Minimum RATA, %	4.56	47.63	61.15	47.65	41.46	8.55

A comparison between the reflector configurations is presented in Fig. 8 for varying array sizes and in Fig. 9 for the RATA.

Tables V and VI show the optimized results with a maximum β of 40° and 20°, respectively. As we can see from those tables, within the investigated azimuth scan range up to ±30°, there is always a situation for each reflector when the entire array is active. Thus, in those tables, the array size is also optimized for minimum dimensions. Table VII contains

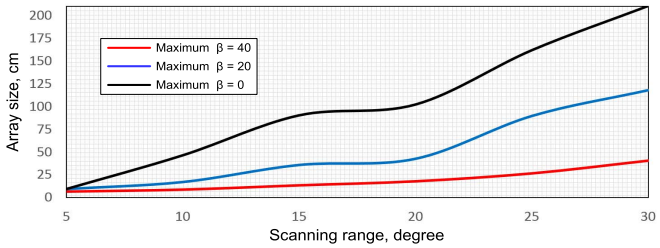

Fig. 8. Array size for the complex offset double-reflector model optimized for EIRP maximization.

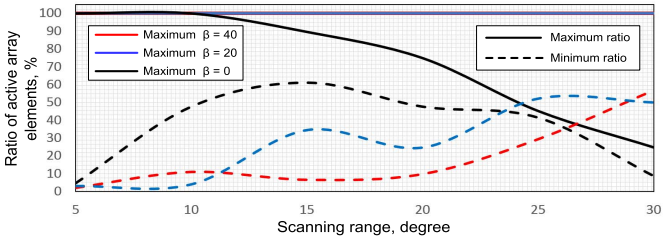

Fig. 9. RATA for the complex offset double-reflector model optimized for EIRP maximization.

the results of the reflector optimization without the possibility of elevation incline. As we can observe, this implies a more challenging situation on the peak EIRP optimization, and only within a limited scan range up to ±10°, it is possible to achieve the situation that all array elements are active for broadside operation. For scan ranges beyond ±10°, the optimization is done only for peak EIRP and does not include the array size minimization.

Similar to the previous optimization, Fig. 8 shows that the required array size is increasing with increased scan range in an almost linear way and with a stricter limit of the maximum β. Moreover, the limit on β limits the optimized peak EIRP as we could see in Fig. 9. For $\beta = 40°$ and $\beta = 20°$, the maximum RATA is equal to 100% for all investigated scan ranges. Whereas for $\beta = 0°$, the maximum RATA is decreasing linearly with increasing azimuth scan range. On the other hand, the minimum RATA is the highest when $\beta = 0°$. This means that the difficulty to achieve the highest peak EIRP is in some way compensated by a higher minimum RATA.

C. Minimum RATA

Within this section, the optimization results for 21 different reflectors configurations toward increasing the minimum RATA are presented. The lowest RATA value within the scan range characterizes how efficient array elements are used. Normally, this parameter is a weak spot of traditional reflector configurations. Classical prime-focused reflectors have a very low RATA while scanning, so most of the array elements remain inactive [24], [25]. The complex offset double-reflector model of [10] allows to have about a quarter of the array elements to be active within a ±20° scan range. Here, we will explore if we can further improve the minimum RATA at the cost of deteriorating other characteristics.

TABLE VIII

OPTIMIZATION RESULTS FOR THE MAXIMIZATION OF THE MINIMUM RATA USING A MULTIVARIABLE GOAL FOR THE COMPLEX OFFSET DOUBLE-REFLECTOR MODEL FOR $\beta = 40°$

	Azimuth scan range n, deg					
	±5	±10	±15	±20	±25	±30
Array size, cm	38.4	28.27	33.3	35.9	41.8	47.2
Maximum RATA, %	99.96	99.04	98.64	99.99	99.61	95.69
Minimum RATA, %	**99.95**	**99.02**	**98.54**	**97.28**	**95.22**	**91.68**

TABLE IX

OPTIMIZATION RESULTS FOR THE MAXIMIZATION OF THE MINIMUM RATA USING A MULTIVARIABLE GOAL FOR THE COMPLEX OFFSET DOUBLE-REFLECTOR MODEL FOR $\beta = 20°$

	Azimuth scan range, deg					
	±5	±10	±15	±20	±25	±30
Array size, cm	37.8	69.4	69.3	95.7	96.4	107.9
Maximum RATA, %	99.86	99.32	98.16	92.98	77.99	99.96
Minimum RATA, %	**99.83**	**99.31**	**98.15**	**82.83**	**70.46**	**56.99**

TABLE X

OPTIMIZATION RESULTS FOR THE MAXIMIZATION OF THE MINIMUM RATA USING A MULTIVARIABLE GOAL FOR THE COMPLEX OFFSET DOUBLE-REFLECTOR MODEL FOR $\beta = 0°$

	Azimuth scan range, deg					
	±5	±10	±15	±20	±25	±30
Array size, cm	85.5	82.5	94.4	141.3	162.2	210.7
Maximum RATA, %	99.96	86.44	75.85	63.85	45.10	24.62
Minimum RATA, %	**99.89**	**84.34**	**72.29**	**59.77**	**41.46**	**8.55**

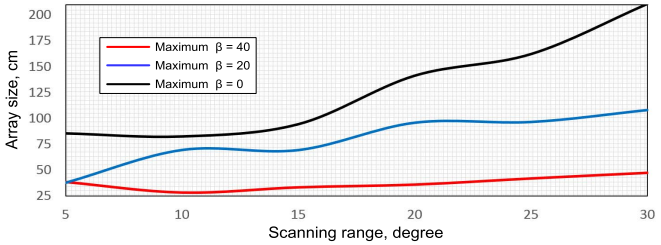

Fig. 10. Array size for the complex offset double-reflector model optimized for maximization of the minimum RATA.

Table VIII contains the optimization results for maximizing the minimum RATA for β limited to 40°, and Tables IX and X for 20° and 0°, respectively.

A comparison between reflector configurations with different limits on β is presented in Fig. 10 for the array size and in Fig. 11 for the RATA.

According to Tables VIII–X, it is not possible to achieve a situation that the entire array remains active within the whole scan range. The minimum RATA is always less than 100% when there is a scan capability realized. Nevertheless, we could see that a dedicated optimization of the complex offset double reflector allows obtaining results radically different from classical prime-focused reflectors. If the prime-focused reflector without reflector elevation incline has an RATA of about 19% for 20° elevation incline [10], the corresponding complex offset double reflector (see Table X) optimized for ±20° scan range has a minimum RATA of almost 60%.

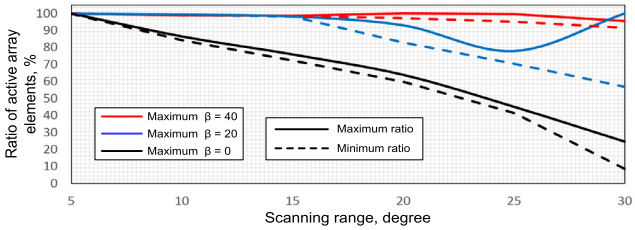

Fig. 11. RATA for the complex offset double-reflector model optimized for maximization of the minimum RATA.

TABLE XI

OPTIMIZATION RESULTS FOR THE MAXIMIZATION OF EIRP AND MINIMUM RATA FOR THE COMPLEX OFFSET DOUBLE-REFLECTOR MODEL FOR $\beta = 40°$

	Azimuth scan range, deg					
	±5	±10	±15	±20	±25	±30
Array size, cm	42.79	50.3	52.66	60.7	48.6	58.23
Maximum RATA, %	**99.97**	**100**	**100**	**100**	**99.99**	**100**
Minimum RATA, %	**99.95**	**99.25**	**96.80**	**96.84**	**95.28**	**91.25**

The costs of the achieved RATA improvement are visible from Fig. 10. The sizes of the required arrays are significantly larger than for other types of optimization. In addition, even for a limited scan range, a larger array is required. For reflectors with an elevation incline up to 40°, the array is almost independent of the scan range. For a strict limit to $\beta = 0°$, the array size remains almost constant up to 15° scan range and then linearly increasing.

The RATA of Fig. 11 demonstrates that up to a 15° scan range, it is possible to keep almost the entire array in active mode for configurations with a maximum β of 20° and 40°. As we know, a β equal to 40° corresponds to a potential loss of directivity of 23.4% and for a β value of 20° to 6%. This fact proves that some compromise toward a potential directivity drop and improvements of the array illumination by the reflector, in terms of a RATA increase, could be done. For β equal to 0°, the maximum and minimum RATA values strongly decrease for wider scan ranges.

D. Maximization of EIRP and the Minimum RATA

As we can see in Section II-C, the optimization of the minimum RATA is leading to the fact that the maximum RATA is also increasing. In addition, the optimization toward peak EIRP is possible using up to 100% of the active array elements for most of the configurations. Thus, it is interesting to combine those goals in one optimization. Both the peak EIRP and the minimum RATA are optimized with equal optimization weight within this paragraph. The optimization outcomes are again presented for 21 different reflectors configurations.

When we look at the results of Section II-B, there is no need for the second-order optimization factor, such as array size minimization in this case. As it has been demonstrated, the minimum RATA never achieves 100% within a nonzero scan range. Thus, the combined goal never could be satisfied fully.

TABLE XII

OPTIMIZATION RESULTS FOR THE MAXIMIZATION OF EIRP AND MINIMUM RATA FOR THE COMPLEX OFFSET DOUBLE-REFLECTOR MODEL FOR $\beta = 20°$

	Azimuth scan range, deg					
	±5	±10	±15	±20	±25	±30
Array size, cm	37.8	69.6	69.7	72.4	82	115.5
Maximum RATA, %	**99.96**	**99.34**	**98.15**	**100**	**100**	**98.08**
Minimum RATA, %	**99.82**	**99.29**	**98.13**	**95.85**	**79.87**	**56.11**

TABLE XIII

OPTIMIZATION RESULTS FOR THE MAXIMIZATION OF EIRP AND MINIMUM RATA FOR THE COMPLEX OFFSET DOUBLE-REFLECTOR MODEL FOR $\beta = 0°$

	Azimuth scan range, deg					
	±5	±10	±15	±20	±25	±30
Array size, cm	90.5	81.1	86	145.5	162.2	210.8
Maximum RATA, %	**99.97**	**99.99**	**81.29**	**61.15**	**45.11**	**24.62**
Minimum RATA, %	**99.89**	**97.96**	**76.00**	**57.39**	**41.46**	**8.56**

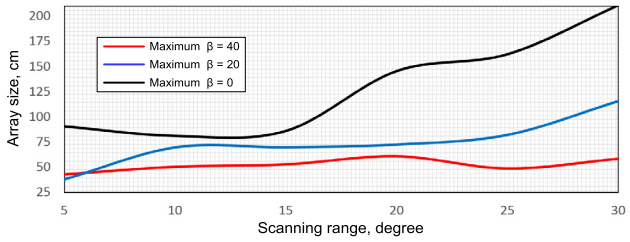

Fig. 12. Array size for the complex offset double-reflector model optimized for maximization of EIRP and minimum RATA.

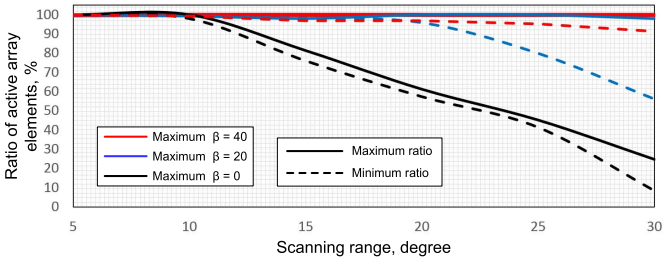

Fig. 13. RATA for the complex offset double-reflector model optimized for maximization of EIRP and minimum RATA.

Table XI contains the optimization results for β limited to 40°, and Tables XII and XIII for 20° and 0°, respectively.

A comparison between reflector configurations with different limits on β is presented in Fig. 12 for array size and in Fig. 13 for the RATA.

As we could see from Tables XI–XIII for the combined goal, the maximum RATA could achieve 100%. This means that within a scan range, there is a certain scan angle when all array elements are going to be involved. For optimization results with a maximum reflector incline angle up to 40° (Table XI), the minimum RATA is also relatively close to 100%. Thus, it is possible to claim that for β maximally equal to 40°, the optimization goal is almost satisfied within the investigated scan range, and it is possible to build an FPA with maximum use of the array elements.

TABLE XIV

OPTIMIZATION RESULTS FOR ARRAY SIZE MINIMIZATION FOR THE COMPLEX OFFSET DOUBLE-REFLECTOR MODEL FOR $\beta = 40°$

	Azimuth scan range, deg					
	±5	±10	±15	±20	±25	±30
Achieved minimum array size, cm	**4.3**	**8.6**	**12.8**	**15.1**	**21.9**	**32.83**
Maximum RATA, %	99.97	99.98	99.98	99.32	99.99	54.07
Minimum RATA, %	17.31	13.97	14.78	27.32	7.54	47.81

TABLE XV

OPTIMIZATION RESULTS FOR ARRAY SIZE MINIMIZATION FOR THE COMPLEX OFFSET DOUBLE-REFLECTOR MODEL FOR $\beta = 20°$

	Azimuth scan range, deg					
	±5	±10	±15	±20	±25	±30
Achieved minimum array size, cm	**6.88**	**12.94**	**26.07**	**40.6**	**75.6**	**108.7**
Maximum RATA, %	99.96	100	53.03	28.06	36.93	57.08
Minimum RATA, %	6.58	4.12	1.68	1.79	32.09	41.05

TABLE XVI

OPTIMIZATION RESULTS FOR ARRAY SIZE MINIMIZATION FOR THE COMPLEX OFFSET DOUBLE-REFLECTOR MODEL FOR $\beta = 0°$

	Azimuth scan, deg					
	±5	±10	±15	±20	±25	±30
Achieved minimum array size, cm	**10.2**	**18.2**	**42.6**	**87.9**	**123.9**	**210.2**
Maximum RATA, %	99.16	88.79	18.82	8.64	28.47	24.55
Minimum RATA, %	3.55	2.96	2.32	1.22	23.67	8.45

Similar to the optimization results of the previous section, the cost of the improvement is the need for a larger overall array size; see Fig. 12. For reflectors with a β of up to 20° and 40°, the array size almost does not depend on the scan range. In the case $\beta = 0°$, the array size remains almost constant up to a 15° scan range and then increases further for wider scan ranges.

According to Fig. 13, the maximum RATA stays almost up to 100% for a ±30° scan range for a maximum β of 40°, within ±20°—for a maximum β of 20° and ±10°—for a maximum β of 0°.

E. Array Size Minimization

From a cost point of view, the most important configuration could be the one that minimizes the overall number of required array elements. In other words, to optimize the shape of the reflector to achieve a minimum array size, it could provide the required performance over the specified scan range. Within this section, the optimization results for 21 different reflectors configurations toward array size minimization are presented.

It is important to notice that the obtained optimization results are scalable with the size of the reflectors and relevant only for the chosen sizes and proportion of the main and sub-reflectors.

Table XIV contains the optimization results of array minimization for β limited to 40°, and Tables XV and XVI for 20° and 0°, respectively.

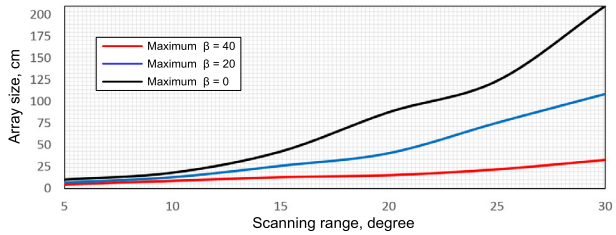

Fig. 14. Array size for the complex offset double-reflector model optimized for array size minimization.

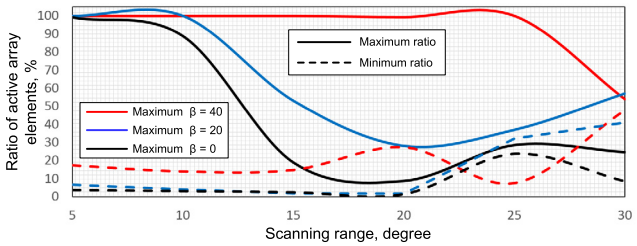

Fig. 15. RATA for the complex offset double-reflector model optimized for array size minimization.

A comparison between reflector configurations with different limits on β is presented in Fig. 14 for the array size and in Fig. 15 for the RATA.

According to Tables XIV–XVI, it is possible to achieve significant array compactness compared with the previous cases. In addition, we could see that dedicated optimization of the complex offset double reflector allows to obtain significantly different array sizes as compared with a similar configuration presented in paper [10] where, for ±20° scanning, an array length of 28 cm length was required. In the dedicated optimization of this section, the configuration with the same β just requires a maximum length of 15.1 cm to provide the same scan range. This is achieved due to the dedicated optimization and due to the larger sub-reflector size up to 1 m, against 83 cm of the paper [10].

The overall optimized array sizes almost increase quadratically with the scan range according to Fig. 14. For smaller scan ranges, the elevation inclines practically do not affect the required array size. However, with the increase in scan range, the difference between configuration limits becomes more pronounced and achieves a ratio of more than 6 for a ±30° scan range between $\beta = 0°$ and $\beta = 40°$.

The RATA of Fig. 15 demonstrates that there are certain scan angles when a significant part of the array will be active. However, the minimum RATA during scanning is significantly reduced compared with the dedicated optimization for RATA maximization (Section II-B). Combined with the factor that optimization toward a compact array also minimizes the overall number of elements, we can conclude that there will be certain scan angles where the number of active elements is really low.

F. Summary of Optimizations

An overview of the required array size for the different optimization goals presented in the previous sections is provided

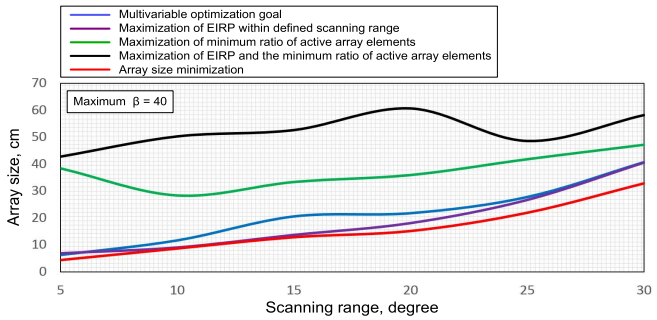

Fig. 16. Array size for the complex offset double-reflector model with β =40° optimized for different goals.

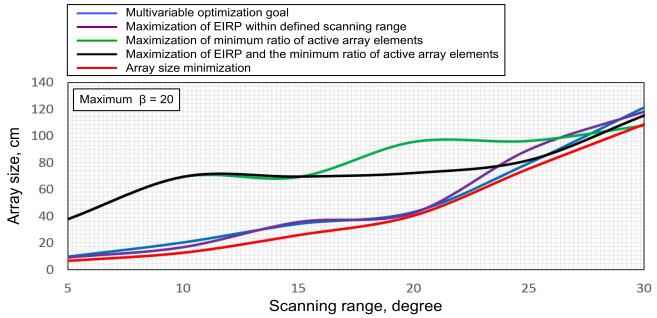

Fig. 17. Array size for the complex offset double-reflector model with $\beta = 20°$ optimized for different goals.

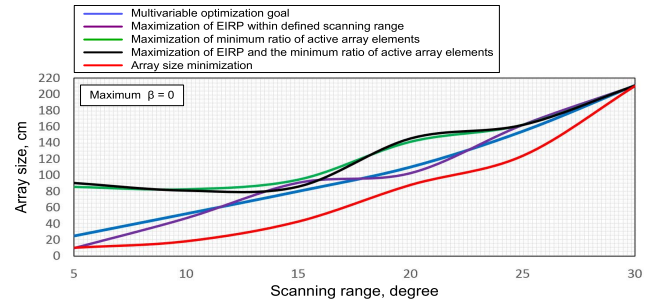

Fig. 18. Array size for the complex offset double-reflector model with $\beta = 0°$ optimized for different goals.

in Fig. 16 for reflector configurations with maximum $\beta = 40°$; see Fig. 17—20°, and Fig. 18—0°, respectively.

As we could see, there is a trade-off between different array characteristics. We could minimize the array size and have more complicated beamforming or have a significant RATA within all scan ranges, but with a relatively large array size. Interesting to notice is that the most significant difference between the required array sizes is observed for cases where the maximum β is equal to 40°; see Fig. 16. For other values of β, it is more difficult to optimize the reflector for a certain optimization goal; see Figs. 17 and 18. Moreover, the increase in the required scan range also minimizes the output optimization results. The required array sizes of Figs. 17 and 18 are becoming the same or almost the same for a scan range of ±30°. Those factors demonstrate that there is a clear limit on reflector designs with improved scanning capabilities.

TABLE XVII
ACHIEVED MINIMUM ARRAY SIZE OF THE COMPLEX OFFSET DOUBLE REFLECTOR FOR DIFFERENT SUB-REFLECTOR SIZES

Achieved minimum array size, cm								
		Dy_s, cm						
		80	85	90	95	100	105	110
Dz_s, cm	15	62.2	64.5	63.6	76.4	85.9	87.3	120.3
	17,5	56.6	74.6	75.0	74.4	69.9	79.2	70.2
	20	41.9	41.9	46.1	35.1	44.5	52.9	42.4
	22,5	29.3	29.4	25.4	29.4	34.6	38.2	44.8
	25	34.4	20.0	16.1	16.5	16.1	18.0	32.8
	27,5	54.3	36.5	35.5	26.7	25.4	18.3	28.8
	30	22.1	21.4	23.9	24.1	18.4	21.1	33.4

Scan ranges wider than ±30° are not advisable, since it is impossible to improve the reflector to obtain acceptable characteristics of the array. In addition, the optimization effect will be significant only if there are compromises on the directivity which the reflectors could provide as compared with classical reflector configurations.

III. ARRAY SIZE MINIMIZATION FOR DIFFERENT SUB-REFLECTOR SIZES

The previously presented optimization results of the array size minimization are relevant for a certain size of the main and sub-reflectors. The size of the main reflector defines the directivity of the whole system. In addition, scaling the main reflector size will cause a scaling of the required sub-reflector and array. The RATA will remain the same. Normally, the main reflector is the bulkiest part of the system and defines the required directivity, while the sub-reflector could be a bit smaller and stretched out in one of the dimensions to provide scan capabilities. Thus, it is interesting to investigate how the sub-reflector size could affect the scan capabilities of the whole system.

Within this section, the optimization results for 49 different reflectors configurations toward array length minimization are presented for different sub-reflector sizes. The investigation is done for a complex offset double-reflector model with a β of 40°. The required scan range has been fixed to ±20° in the azimuth plane. In the orthogonal non-scanning plane, the width of the array has been fixed to 4 cm. The sub-reflector sizes Dy_s vary from 80 to 110 cm in the scanning plane and Dz_s from 15 to 30 cm in the orthogonal plane.

The optimization results of the array size minimization are presented in Table XVII, the maximum RATA in Table XVIII, and the minimum RATA in Table XIX.

According to Table XVII, there is an optimum size of the sub-reflector for a defined reflector specification. We could see that the minimum array size is achieved with a sub-reflector size of 90–100 cm in the scan plane and 25 cm in the orthogonal plane. Both dimensions are affecting the achieved size of the array. In addition, from Table XVII, we can see the limitation of Dz_s, which has a significant effect on the array size. It is also important to notice that a further increase in the dimensions of the sub-reflectors does not help to minimize the array size further.

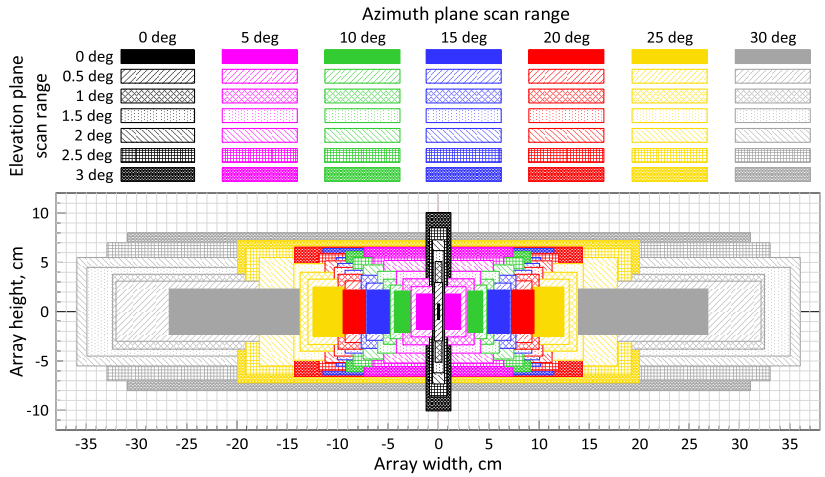

Fig. 19. Array size for 2-D scanning with the complex offset double reflector. Azimuth scan range up to ±30° and elevation scan range up to ±3°.

TABLE XVIII

MAXIMUM RATA OF THE COMPLEX OFFSET DOUBLE-REFLECTOR MODEL FOR DIFFERENT SUB-REFLECTOR SIZES

Maximum RATA, %								
		Dy_s, cm						
		80	85	90	95	100	105	110
Dz_s, cm	15	11.69	16.37	18.35	22.59	28.48	30.99	44.75
	17.5	11.35	27.64	26.69	24.38	25.31	48.91	51.93
	20	45.75	18.45	13.84	46.82	33.01	42.98	24.93
	22.5	34.66	43.01	35.17	23.99	12.82	21.03	30.62
	25	45.21	79.49	75.59	99.99	99.88	99.99	11.53
	27.5	21.99	50.97	21.87	42.70	49.93	99.99	41.59
	30	98.13	99.99	99.99	99.98	99.98	100	52.95

TABLE XIX

MINIMUM RATA OF THE COMPLEX OFFSET DOUBLE REFLECTOR FOR DIFFERENT SUB-REFLECTOR SIZES

Minimum RATA, %								
		Dy_s, cm						
		80	85	90	95	100	105	110
Dz_s, cm	15	7.30	10.23	11.66	15.52	16.77	16.48	44.26
	17.5	5.92	23.34	24.32	15.71	18.49	26.32	12.32
	20	7.29	10.29	3.72	11.80	2.05	1.38	0.98
	22.5	21.18	13.58	21.99	4.12	3.52	2.13	3.62
	25	4.84	7.35	41.53	9.53	3.21	2.29	6.84
	27.5	4.84	11.56	8.68	11.39	4.69	1.49	15.12
	30	32.30	9.22	19.66	17.11	13.30	3.24	25.50

The maximum RATA (Table XVIII) depends on the sub-reflector size in a straightforward way. With increasing sub-reflector size, the maximum number of simultaneously involved elements within the defined scan range is also increasing. It is achieving almost 100% for a maximum Dz_s of 30 cm. The minimum RATA (Table XIX) in its turn has a mixed dependence. However, some of the sub-reflector sizes achieve a minimum RATA of up to 40%. For example, one of the smallest achieved arrays corresponded to a Dz_s equal to 25 cm and a Dy_s equal to 90 cm.

IV. ARRAY SIZE MINIMIZATION FOR 2-D SCANNING

Next to scanning in the azimuth plane, scanning in elevation could be very useful, for example, to compensate for antenna tower vibrations due to wind, which could lead to a beam misalignment of a few degrees [15]. Thus, in addition to the wide-scan capabilities in the azimuth plane, it is crucial to have a limited scanning functionality in the opposite orthogonal plane. In the previous paragraph, we have seen that the sizes of both sub-reflectors affect the minimum required array size.

Within this section, the optimization results for 49 different reflectors configurations toward array size minimization are presented for scanning in two planes. Similar to the previous cases, the scanning in azimuth is investigated in the range of up to ±30°. In the orthogonal elevation plane, the scan range is limited to ±3°. The investigation is done for a complex offset double reflector with $\beta = 40°$. The sub-reflector size is 100 × 45 cm. The desired array size is minimized in the main scanning plane and remains equal to 4 cm in the elevation plane.

Table XX presents the optimization results of the array size and associated dimensions. Fig. 19 presents a comparative analysis of the minimum required array size for different scan ranges in azimuth and elevation. The maximum RATA is presented in Table XXI, and the minimum RATA in Table XXII.

According to Table XX, as has been expected, the minimum required array size strongly depends on the scanning requirements in both planes. We can observe in Fig. 19 that scanning in the elevation plane makes the array size minimization much more challenging. For example, for scanning up to ±20° in the azimuth plane (red color in Fig. 19), the required array size is significantly larger in both dimensions if there is scanning in the elevation plane. For 0° scan in elevation, the array size is 19 × 4.4 cm, whereas for ±3°, we obtain a size of 28.6 × 13.1 cm. The main reason is the difficulty to avoid blockage when we scan in the elevation plane. In addition, the focusing properties of the reflectors are sacrificed for wider scanning. The overall shapes of the reflector are more stretched in the

TABLE XX
ACHIEVED MINIMUM ARRAY SIZE FOR THE COMPLEX OFFSET DOUBLE-REFLECTOR MODEL FOR 2-D SCANNING

Achieved minimum array size, length, cm, width cm, area, cm^2								
		Azimuth scan range, deg						
		0	±5	±10	±15	±20	±25	±30
Elevation scan range, deg	0	0.1x3.1 0.3	4.4x3.6 15.5	8.9x4.1 36.5	14.2x4.5 64.1	19x4.4 83.9	25.1x5.2 129	53.7x4.7 253
	±0.5	0.8x5.9 4.5	5.5x5.1 27.8	9.7x5.4 52.7	14.5x5.8 83.4	18.6x6.4 118.5	25.9x6.7 174.8	64.5x6.1 396.0
	±1	0.7x10.1 6.8	7.2x6.6 47.8	10.9x6.7 73.7	15.4x7.4 113.7	19.6x7.7 150.7	27.5x8.1 222.7	64.9x7.6 498.0
	±1.5	1.1x12.4 13.5	8.5x8.2 69.1	12.1x8.2 98.8	18.7x8.4 158.3	20.7x9 186.4	28.7x9.8 282.8	69.4x9.1 634.0
	±2	1.3x14.7 19.7	11x10.4 114.9	15.3x9.5 145.6	20.3x9.8 198.8	22.7x10.5 237.6	35.6x11 391.3	71.1x10.8 771.0
	±2.5	1.9x17.2 32.5	13.3x11.4 151.5	17.1x10.8 185.7	21.7x11.1 241.3	24.1x11.8 286.4	38.4x12.8 490.8	65.7x13.3 876.0
	±3	2.5x20.1 49.9	14.8x13 192.9	18.4x12.2 224.3	22.9x12.6 290.0	28.6x13.1 374.6	39.5x14.5 573.0	61.8x15.5 961.0

TABLE XXI
MAXIMUM RATA OF THE COMPLEX OFFSET DOUBLE REFLECTOR FOR 2-D SCANNING

Maximum RATA, %								
		Azimuth scan range, deg						
		0	±5	±10	±15	±20	±25	±30
Elevation scan range, deg	0	100	95.75	91.08	80.48	79.93	76.43	77.48
	±0.5	62.56	69.44	71.11	64.84	61.45	57.94	40.65
	±1	58.34	55.82	59.04	53.34	53.01	48.56	30.78
	±1.5	49.41	47.63	50.81	35.10	47.47	40.94	30.45
	±2	42.42	28.49	34.57	33.26	41.97	34.25	26.02
	±2.5	39.47	26.11	29.59	30.66	38.63	28.51	23.96
	±3	36.67	24.40	28.41	27.46	25.22	23.70	17.78

TABLE XXII
MINIMUM RATA OF THE COMPLEX OFFSET DOUBLE REFLECTOR FOR 2-D SCANNING

Minimum RATA, %								
		Azimuth scan range, deg						
		0	±5	±10	±15	±20	±25	±30
Elevation scan range, deg	0	100	34.26	20.75	11.81	10.24	20.78	51.91
	±0.5	46.58	14.14	9.94	5.23	5.59	10.65	28.20
	±1	43.17	6.50	6.77	6.39	5.35	5.29	20.84
	±1.5	34.54	5.63	7.26	3.62	3.94	2.54	17.29
	±2	26.89	4.95	3.18	2.85	3.15	6.91	12.69
	±2.5	22.79	6.53	2.37	2.28	2.46	3.27	8.82
	±3	20.63	5.23	1.95	1.76	1.58	1.36	5.19

azimuth plane where the main scanning is provided. Moreover, according to Table XX, a larger array size is required for an increased scan range in each of the planes.

The maximum RATA (Table XXI) depends quite straightforward on the scan requirements. As could be expected for zero scan in both planes, all array elements are all-time active. With increasing scan range, the maximum RATA is gradually decreasing and achieves a minimum for the widest scan ranges in both planes.

The minimum RATA (Table XXII) has a maximum value for the non-scanning cases. For other situations, it is significantly lower and demonstrates that most of the array elements are not involved in 2-D scanning. The most challenging situation occurs for an elevation scan range up to ±3°. In this case, the RATA drops to a few percent due to the significant beam deviation and limited focusing properties in the offset plane.

TABLE XXIII
MAIN REFLECTOR SHAPE OF THE COMPLEX OFFSET DOUBLE REFLECTOR FOR 2-D SCANNING. "H" STANDS FOR A HYPERBOLIC SHAPE, AND "P" STANDS FOR A PARABOLIC SHAPE

Main reflector shape								
		Azimuth scan range, deg						
		0	±5	±10	±15	±20	±25	±30
Elevation scan range, deg	0	H	P	P	P	H	P	P
	±0.5	H	P	P	P	H	P	P
	±1	H	P	P	P	P	H	P
	±1.5	H	H	H	H	P	H	H
	±2	H	H	H	H	P	H	P
	±2.5	H	H	P	P	P	P	P
	±3	H	P	P	P	P	P	P

TABLE XXIV
SUB-REFLECTOR SHAPE OF THE COMPLEX OFFSET DOUBLE REFLECTOR FOR 2-D SCANNING. "H" STANDS FOR A HYPERBOLIC SHAPE, AND "P" STANDS FOR A PARABOLIC SHAPE

Sub-reflector shape								
		Azimuth scan range, deg						
		0	±5	±10	±15	±20	±25	±30
Elevation scan range, deg	0	H	H	H	H	H	P	H
	±0.5	H	H	H	H	H	P	H
	±1	H	H	H	H	H	P	H
	±1.5	H	H	H	H	H	H	H
	±2	H	H	H	H	H	H	H
	±2.5	H	H	H	H	H	H	P
	±3	H	H	H	H	H	H	P

Traditionally, the parabolic shape is considered the most common type of surface for classical prime focus reflectors [26]. It is also well known that a spherical reflector could provide a minimum beam deviation during scanning [6]. Nevertheless, the situation for the investigated complex offset double reflector is more complicated. The main reflector shape for different scan ranges is presented in Table XXIII, and for the sub-reflector in Table XXIV.

From Tables XXIII and XXIV, we could see that parabolic reflector shapes are not always the optimal solutions. It really depends on the scanning requirements. For the main reflector, the parabolic shape has a mixed variation of hyperbolic and parabolic shapes, whereas the optimal shape of the sub-reflector is always a hyperbolic shape.

V. Conclusion

Within this article, a detailed analysis of FPA configurations has been presented in terms of technology limits for wide-angle scanning. It has been shown how different optimizations could allow building systems with various performances in terms of the key operating parameters, such as array size, EIRP, and the RATA.

It is possible to improve the best-case operation or create configurations where the entire array is active for a certain scan angle, with a maximum RATA of 100%. For instance, reflector configurations can be obtained with all elements active for broadside operation. At the same time, these configurations are capable to provide scanning within the defined range at the expense of a much lower RATA.

For improving the overall array performance, we only optimize the minimum RATA or improve the RATA over the whole scan range. The minimum RATA is always well below 100% when there is a scan capability realized. Nevertheless, we have shown that this parameter can be significantly improved using optimization. The proposed double reflector is optimized for a $\pm 20^\circ$ scan range and provides a minimum RATA of almost 60%, while for classical prime-focused reflectors, this is equal to 19% only.

It is also possible to significantly reduce the required array size by a dedicated optimization. With a size of the main reflector of 80 cm, the minimum array size to provide $\pm 20^\circ$ azimuth scanning is equal to 15.1×4 cm, while for a classical prime-focused reflector, the array size is 52×9 cm (the latter was presented in [10]). The required minimum array size is significantly larger in both dimensions when we also require additional scanning in the elevation plane.

The ratio between the main and sub-reflector can also be subject to optimization. We have shown that there are optimum dimensions of the sub-reflector in order to achieve a minimum array size.

Overall, it has been shown that there is a trade-off between different FPA characteristics. It is possible to minimize the array size and, at the same time, have a smaller number of active array elements or have a significant RATA within all scan ranges, but with a relatively large array size.

References

[1] P. Benthem et al., "Aperture array development for future large radio telescopes," in *Proc. 5th Eur. Conf. Antennas Propag. (EUCAP)*, May 2011.

[2] A. Zamanifekri and A. B. Smolders, "Optimum configuration of focal plane arrays for satellite communication," in *Proc. IEEE Antennas Propag. Soc. Int. Symp. (APSURSI)*, Jul. 2013, pp. 952–953.

[3] E. Brookner, "Phased array radars-past, present and future," in *Proc. RADAR*, 2002, pp. 104–113.

[4] S. Shu, S. R. Theodore, S. Mansoor, T. Pan, Z. Jianhua, and J. S. Peter, "Propagation models and performance evaluation," *IEEE Trans. Veh. Technol.*, vol. 67, no. 9, pp. 8422–8439, Sep. 2018.

[5] U. Johannsen, T. A. H. Bressner, A. Elsakka, A. B. Smolders, and M. Johansson, "Base station antenna systems for mm-waves," in *Proc. Int. Symp. Antennas Propag. (ISAP)*, Jan. 2021, pp. 593–594.

[6] A. Dubok, A. Al-Rawi, M. H. A. J. Herben, G. Gerini, and A. B. Smolders, "Wide-angle scanning reflector configuration for focal plane arrays," in *Proc. IEEE Int. Symp. Antennas Propag. (APSURSI)*, Jun. 2016, pp. 1625–1626.

[7] F. Pelorossi, G. Toso, and P. Angeletti, "On the scanning properties of imaging antennas based on dual confocal paraboloidal reflectors," *Prog. Electromagn. Res. M*, vol. 37, pp. 95–107, 2014.

[8] A. Dubok et al., "Double-reflector configuration for optimal exposure of wideband focal-plane arrays with optical beamforming," *IEEE Trans. Antennas Propag.*, vol. 65, no. 8, pp. 4316–4321, Aug. 2017, doi: 10.1109/TAP.2017.2709620.

[9] A. Dubok, A. Al-Rawi, G. Gerini, and A. B. Smolders, "Extreme scanning focal-plane arrays using a double," *Trans. Antennas Propagation. Commun.*, vol. 68, no. 7, pp. 5686–5690, 2020.

[10] A. Dubok, A. Al-Rawi, G. Gerini, and A. B. Smolders, "Reflector synthesis for wide-scanning focal plane arrays," *IEEE Trans. Antennas Propag.*, vol. 67, no. 4, pp. 2305–2319, Apr. 2019.

[11] G. Toso, "The beauty of multibeam antennas," in *Proc. 9th Eur. Conf. Antennas Propag. (EUCAP)*, Lisbon, Portugal, Apr. 2015, pp. 12–17.

[12] M. N. M. Kehn and L. Shafai, "Characterization of dense focal plane array feeds for parabolic reflectors in achieving closely overlapping or widely separated multiple beams," *Radio Sci.*, vol. 44, no. 3, pp. 1–25, Jun. 2009.

[13] A. Al-Rawi, A. Dubok, S. J. Geluk, B. P. de Hon, M. H. A. J. Herben, and A. B. Smolders, "Increasing the EIRP by using FPA-fed reflector antennas," in *Proc. IEEE Int. Symp. Antennas Propag. (APSURSI)*, Jun. 2016, pp. 1623–1624.

[14] A. B. Smolders et al., "Building 5G millimeter-wave wireless infrastructure: wide-scan focal-plane arrays with broadband optical beamforming," *IEEE Antennas Propag. Mag.*, vol. 61, no. 2, pp. 53–62, Apr. 2019.

[15] A. Al-Rawi, A. Dubok, M. H. A. J. Herben, and A. B. Smolders, "Point-to-point radio link variation at E-band and its effect on antenna design," in *Prog. Electromagn. Res. Symp.*, Jul. 2015, pp. 913–917.

[16] A. Al-Rawi, A. Dubok, S. J. Geluk, M. H. A. J. Herben, and A. B. Smolders, "A comparative study on the parabolic and spherical FPA-fed reflector antenna," in *Proc. 10th Eur. Conf. Antennas Propag. (EuCAP)*, Apr. 2016, pp. 1–4.

[17] A. H. Guenther, L. S. Pedrotti, and C. Roychoudhuri, *Fundamentals of Photonics*. Waco, TX, USA: Univ. Connecticut, 2000.

[18] F. J. S. Moreira and J. R. Bergmann, "Classical axis-displaced dual-reflector antennas for omnidirectional coverage," *IEEE Trans. Antennas Propag.*, vol. 53, no. 9, pp. 159–163, Sep. 2005.

[19] B. S. Westcott, F. A. Stevens, and F. Brickell, "GO synthesis of offset dual reflector," *IEE Proc. H-Microw., Opt. Antennas*, vol. 128, no. 1, pp. 11–18, 1981.

[20] B. S. Westcott, F. A. Stevens, and F. Brickell, "GO synthesis of offset dual reflector," *IEE Proc. H-Microw., Opt. Antennas*, vol. 128, no. 1, pp. 11–18, 1981.

[21] S. G. Hay, "A double-edge-diffraction Gaussian-series method for efficient physical optics analysis of dual-shaped-reflector antennas," *IEEE Trans. Antennas Propag.*, vol. 53, no. 8, pp. 2597–2610, Aug. 2005.

[22] D. B. Hayman, T. S. Bird, K. P. Esselle, and P. Hall, "Encircled power study of focal plane field for estimating focal plane array size," in *Proc. IEEE Antennas Propag. Soc. Int. Symp.*, vol. 3A, Jul. 2005, pp. 371–374.

[23] *TICRA Software*. [Online]. Available: https://www.ticra.com/software/grasp/

[24] D. B. Hayman, T. S. Bird, K. P. Esselle, and P. Hall, "Encircled power study of focal plane field for estimating focal plane array size," in *Proc. IEEE Antennas Propag. Soc. Int. Symp.*, vol. 3A, Jul. 2005, pp. 371–374.

[25] M. Zimmerman, S. W. Lee, B. Houshmand, Y. Rahmat-Samii, and R. Acosta, "A comparison of reflector antenna designs for wide-angle scanning," in *Proc. ASA Technical Memorandum*. Hampton, VA, USA: NASA Technology Workshop for Earth Science Geostationary Platforms, Sep. 1988.

[26] H. C. Minnett and B. M. Thomas, "Fields in the image space of symmetrical focusing reflectors," *Proc. Inst. Electr. Eng.*, vol. 115, no. 10, p. 1419, 1968.

Aleksei Dubok was born in Pskov, Russia, in 1987. He received the bachelor's and master's degrees *(cum laude)* in microwave, optical, and digital means of telecommunications from Saint Petersburg State Electrotechnical University, Saint Petersburg, Russia, in 2008 and 2010, respectively, the master's degree in electrical engineering and power electronics from the Lappeenranta University of Technology, Lappeenranta, Finland, in 2011, the Professional Doctorate in Engineering degree in information and communication technology from the Eindhoven University of Technology, Eindhoven, The Netherlands, in 2013, and the Ph.D. degree in electrical engineering from the Eindhoven University of Technology in 2017, with a focus on planar reflector phased array antenna for multiple applications.

From 2007 to 2010, he was an Engineer Developer of communications systems with TELROS Integration, Saint Petersburg. The research has been focused on the design of an antenna-in-package solution for RFID tags. Since 2017, he has a Guest Researcher with the Eindhoven University of Technology and an RF Designer with Philips, Amsterdam, The Netherlands, where he has been involved in the field of RF hardware development and patient safety for MRI. His main research interests include phased arrays antennas, reflector antennas, frequency selective surfaces, SAR and RF safety, near-field interaction, and electromagnetic compatibility. The main application fields of interest are wireless communications, telecommunication systems, imaging, and RF applications in medicine.

A. Bart Smolders (Senior Member, IEEE) was born in Hilvarenbeek, The Netherlands, in 1965. He received the M.Sc. and Ph.D. degree in electrical engineering from the Eindhoven University of Technology (TU/e), Eindhoven, The Netherlands, in 1989 and 1994, respectively.

From 1989 to 1991, he was an IC Designer with FEL-TNO, The Hague, The Netherlands. From 1994 to 1997, he was a Radar System Designer with Thales, Hengelo, The Netherlands. From 1997 to 2000, he was a Project Leader of the Square Kilometer Array (SKA) with the Netherlands Foundation for Research in Astronomy (ASTRON), Dwingeloo, The Netherlands. From 2000 to 2010, he has been with NXP (formerly Philips) Semiconductors, Amsterdam, The Netherlands, responsible for the innovation in the RF business line. Since 2010, he has been a full-time Professor with the Electromagnetics Group, TU/e, with a special interest in antenna systems and applications. He is also the Dean of the Electrical Engineering Department, TU/e. He currently leads several research projects in the area of integrated antenna systems operating at the frequencies up to 120 GHz for several application domains, including 5G/6G wireless communications, radar sensors, and radio astronomy. He has authored or coauthored more than 140 papers.

Dr. Smolders is a Board Member of the Stichting Wetenschappelijke Activiteiten van het Nederlands URSI Committee (SWAN) and a member of the Advisory Board of ASTRON. He is the Junior-Past Chairman of the IEEE Benelux Section and the Past-Chair of the Nederlands Elektronica en Radio Genootschap (NERG).